Available online at www.sciencedirect.com
ScienceDirect
International Journal of Mass Spectrometry 265 (2007) 187–196
International Journal of Mass Spectrometry
www.elsevier.com/locate/ijms

Molecular beads on a charged molecular string: α,ω-alkyldiammonium complexes of cucurbit[6]uril in the gas phase

Haizhen Zhang, Tyler A. Ferrell, Matthew C. Asplund, David V. Dearden *

Department of Chemistry & Biochemistry, C100 Benson Science Building, Brigham Young University, Provo, UT 84602-5700, USA

Received 31 October 2006; received in revised form 27 January 2007; accepted 7 February 2007
Available online 11 February 2007

Abstract

Complexes of α,ω-alkyldiammonium cations $[H_3N^+(CH_2)_nNH_3^+$, $n = 2$–10] with the cyclic, hollow ligand cucurbit[6]uril (CB6) were characterized in the gas phase using Fourier transform ion cyclotron resonance mass spectrometry with energy resolved sustained off-resonance irradiation (SORI) collision induced dissociation, in combination with HF/6-31G* and B3LYP/6-31G* computational methods. All the complexes have the diammonium cation threaded through the cavity of CB6. The modeled supramolecular geometries, the SORI energies required for dissociation of the complexes and for appearance of singly protonated diamine product ions, and the branching ratios for the various dissociation channels all suggest that the optimum α,ω-alkyldiammonium chain length for binding CB6 in the gas phase occurs for $n = 4$. This contrasts with observed complex stability constants in aqueous formic acid, which are maximum for $n = 6$, reflecting solvent stabilization of the ammonium groups that is not possible in the gas phase. At the B3LYP/6-31G* level of theory, the binding energy for the $n = 4$ complex with respect to dissociation to singly protonated butanediamine and protonated CB6 is 204 kJ mol^{-1}. The $n = 6$ complex exhibits especially low dissociation thresholds, perhaps reflecting compression of the diammonium cation upon complexation with CB6, forming a loaded "molecular spring."

Keywords: SORI; Alkyldiamine; Cucurbituril

1. Introduction

Molecular nanotechnology [1], the development and application of devices of nanometer size built from single molecules or supramolecular assemblies of a few molecules, is one of the most promising new areas of 21st century research. Most researchers in the nanotechnology area have taken the approach of making existing devices smaller (for example, decreasing the size of transistors used in microchips) or of carrying out existing processes on a smaller scale (for instance, using shorter wavelength radiation to scale down photolithography). Another approach, one favored by nature, is to redesign the devices using the smallest possible components, atoms and molecules. The feasibility of this approach is demonstrated in biology; biological systems use extensive molecule-based "nanotechnology," with DNA acting as a molecular information storage device and various proteins serving as molecular machines.

With the push to design and synthesize artificial nanodevices comes an urgent need to develop techniques for characterizing them. Most current methods focus on imaging the nanodevices, usually on surfaces, with high (preferably atomic) resolution. While imaging techniques are powerful, they suffer from limitations in their ability to chemically characterize the materials being imaged. In addition to imaging, techniques typically used to characterize nanomaterials and supramolecular assemblies include NMR, UV-vis and IR spectroscopy, thermogravimetry, X-ray crystallography, and electrospray mass spectrometry (ESI-MS) [2,3]. If the molecules of interest contain paramagnetic atoms or undergo rapid exchange/equilibration among multiple structures, NMR will be of only limited value. In addition, it is often difficult to obtain crystals of sufficient quality for X-ray structure determination. ESI-MS is primarily used only for detection of the molecular ion corresponding to a supramolecular structure, but seldom is it used for structural characterization beyond this. Of these methods, all but ESI-MS require relatively large amounts of material, and all (including ESI-MS as it is usually practiced) are strongly influenced by the presence of solvent

* Corresponding author. Tel.: +1 801 422 2355; fax: +1 801 422 0153.
E-mail address: david_dearden@byu.edu (D.V. Dearden).

1387-3806/$ – see front matter © 2007 Elsevier B.V. All rights reserved.
doi:10.1016/j.ijms.2007.02.002

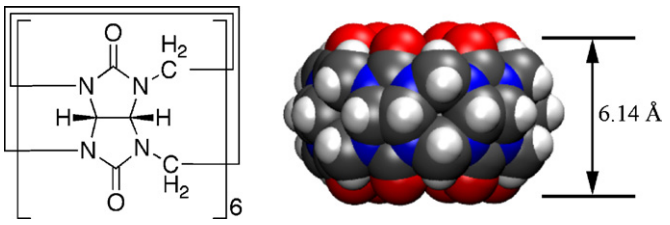

Fig. 1. Structural and space filling models of cucurbit[6]uril, CB6.

or other matrix materials. Thus, an urgent need exists for new analytical methods.

Cucurbiturils [4] are pumpkin-shaped cyclic polymers of glycoluril with hollow interior cavities that are promising as components of supramolecular devices. As shown in Fig. 1, carbonyl oxygen atoms line the portals of the cucurbituril and form ideal binding sites for positive ions, while the interior cavities can contain neutral molecules of proper size. Cucurbiturils composed of n glycoluril units are named cucurbit[n]urils, CBn hereafter.

CB6 has been known for over 100 years, and has been extensively characterized in condensed media beginning in the 1980s [4]. CB6 is of the proper size to form complexes with α,ω-alkyldiammonium cations in solution. In condensed media, these complexes have rotaxane structures, where the diammonium chain is threaded through the cucurbituril. Despite its low solubility in most solvents, CB6 and its complexes are straightforward to study using ESI-MS, and provide a good test bed for new mass spectrometric methods for characterizing supramolecular assemblies.

We recently used complexes of 1,4-diaminobutane with CB6 to demonstrate that ESI-MS sample introduction, combined with tandem mass spectrometry, can be used to distinguish between threaded, rotaxane structures and non-threaded conformations [5]. Both the reactivity of these complexes with neutral amines and their collision induced dissociation (CID) behavior are distinct. Threaded structures react with propylamine via slow addition, whereas non-threaded structures react via rapid amine exchange. Threaded complexes are relatively difficult to dissociate collisionally and tend to do so via covalent cleavages, whereas non-threaded structures tend to dissociate via disruption of the non-covalent interactions between the assembled molecules.

In this paper we explore the collisional dissociation behavior of α,ω-alkyldiammonium ion $[H_3N^+(CH_2)_nNH_3^+, n = 2–10]$ complexes of CB6 in much greater detail, using sustained off-resonance irradiation (SORI) CID techniques [6], which have recently been reviewed [7]. We apply SORI in an energy-resolved manner to characterize fragmentation as a function of energy and the relative binding strengths of the various complexes, with an eye toward determining the intrinsic optimum alkyldiammonium chain length for binding CB6.

With the increasing availability of more powerful computers, even supramolecular complexes consisting of more than 80 heavy atoms, such as those described here, are within the reach of reasonably accurate computational methods. Computational chemistry, which excels at the description of isolated molecules in the gas phase, is an ideal complement to the gas phase experiments described in this paper, and we employ computational methods extensively to supplement and illuminate our experimental studies.

2. Experimental

2.1. Instrument

All experiments were carried out using a Bruker model APEX 47e FT-ICR mass spectrometer controlled by a MIDAS data system [8] and equipped with a microelectrospray source modified from an Analytica design, with a heated metal capillary drying tube based on the design of Eyler [9].

2.2. Materials

CB6 and n-alkyldiamines ($n = 2–10$) were purchased from Sigma Chemical Co. (St. Louis, MO) and used without further purification. CB6 was dissolved in 88% formic acid (Fisher Scientific, New Jersey), diluted to about 1 mM in 50:50 methanol/water, and mixed with about 2 mM n-alkyldiamine. The samples were electrosprayed at a typical flow rate of 10 μL/h.

2.3. SORI–CID experiments

Stored waveform inverse Fourier transform [10] techniques were used to isolate target peaks. Sustained off-resonance irradiation–collision-induced dissociation (SORI–CID) [6] experiments were performed by irradiating 1 kHz below the resonant frequency of the ion of interest. Collision gas (air) was introduced using a Freiser-type pulsed leak valve [11], which maintains a constant pressure during the SORI excitation. SORI events involved pulsing the background pressure in the trapping cell up to 10^{-5} mbar and applying the off-resonance irradiation for 5 s. The amplitude of the SORI RF pulse was varied programmatically through a range of values from less than the threshold for dissociation to several times the threshold value. Ten scans were averaged for each SORI amplitude.

2.4. Threshold data analysis

Data analysis was performed with a modified version of the MIDAS Analysis software package [8] that was capable of extracting peak amplitudes from a set of spectra that differ in one or more experimental parameters (in this case, SORI amplitude). The software generated tables of peak intensities as a function of SORI excitation voltage.

Meaningful comparison of SORI data for different molecular systems requires a relationship between SORI amplitude and the amount of energy supplied to the molecular system by the SORI process. Because SORI supplies energy to the parent ion via a series of low energy collisions, both the average collision energy and the total number of collisions contribute to the total energy available, E_{SORI} [12]. E_{SORI} is the product of the number of collisions the parent ion undergoes, n_{coll}, and the average

energy transferred per collision in the center-of-mass frame of reference, E_{coll}:

$$E_{SORI} = n_{coll} E_{coll} \quad (1)$$

The number of collisions the ion undergoes is a function of the collision frequency, ν_{coll}, and the time during which collisions take place, t_{coll} (the length of the SORI event):

$$n_{coll} = \nu_{coll} t_{coll} \quad (2)$$

The product of neutral gas number density, N^*, collision cross section, σ, and ion velocity, v, gives the collision frequency:

$$\nu_{coll} = N^* \sigma v \quad (3)$$

The maximum kinetic energy in the center-of-mass reference frame during SORI, E_{CM}^{max}, has been derived by Laskin and Futrell [13]. In the following expression, β is the trapping cell geometry factor, q is the charge on the ion, d is the trapping cell diameter, Δf is the frequency offset of the excitation pulse from the ion's resonant frequency, M is the mass of the neutral, m is the mass of the ion, and V_{pp} is the peak-to-peak amplitude of the SORI excitation pulse.

$$E_{CM}^{max} = \frac{\beta^2 q^2}{32\pi^2 d^2 (\Delta f)^2} \left(\frac{M}{M+m} \right) \frac{V_{pp}^2}{m} \quad (4)$$

The maximum kinetic energy in the center of mass frame is also related to the maximum velocity of the activated ions, v_{max}, and reduced mass, μ:

$$E_{CM}^{max} = \frac{1}{2} \mu v_{max}^2 \quad (5)$$

Combining Eqs. (4) and (5), we derive an expression for the maximum ion velocity during the SORI event:

$$v_{max} = \frac{\beta q}{4\pi d (\Delta f)} \frac{V_{pp}}{m} \quad (6)$$

We assume that the average ion velocity, v, is proportional to v_{max} and much greater than the thermal velocity of the neutral collision partner. The following expression for n_{coll} results, where K_v is the proportionality constant relating v to v_{max}:

$$n_{coll} = N^* \sigma K_v \frac{\beta q}{4\pi d (\Delta f)} \frac{V_{pp}}{m} t_{coll} \quad (7)$$

Absent knowledge of the kinetic-to-internal energy deposition function, we assume a constant fraction of the maximum kinetic energy, f_E, is deposited into the ion; for systems where detailed studies have been made [13,14], this is approximately correct. Combining Eqs. (1), (4) and (7), we arrive at an expression for the amount of energy deposited in the ion via the SORI event:

$$E_{SORI} = N^* \sigma K_v f_E t_{coll} \frac{\beta^3 q^3}{128\pi^3 d^3 (\Delta f)^3} \left(\frac{M}{M+m} \right) \frac{V_{pp}^3}{m^2} \quad (8)$$

In our experiments, all the terms in Eq. (8) are constant except σ, M, m, and V_{pp}. Therefore, it follows that E_{SORI} is proportional to the experimental parameters as expressed in Eq. (9):

$$E_{SORI} \propto \sigma \left(\frac{M}{M+m} \right) \frac{V_{pp}^3}{m^2} \quad (9)$$

We assume collision cross sections to be independent of velocity (the hard sphere collision limit). Relative collision cross sections were estimated by computing the solvent accessible surface areas of the various complexes using a probe radius of 1.5 Å; the maximum variation from smallest to largest complex was less than 8.5%. The relative energy scales for the various SORI processes were determined using Eq. (9), with no attempt at quantitative calibration.

Relative thresholds were extracted by linear fitting to the rising portion of the fragment ion curve and extrapolation to the x-intercept of the fitted line. As we note below, FTICR discriminates against low mass fragment ions, and it is possible such discrimination might affect the positions of the measured thresholds. We believe such effects are likely to be small because the high mass fragment ions from the various parent complexes all have similar masses (varying in general by less than 10%). If discrimination were strongly influencing the positions of the thresholds, we would expect to see systematic variation in the thresholds as mass varies, but such systematic effects are not observed. Therefore, we have made no attempt to correct the data for potential mass discrimination effects, which at this juncture remain poorly understood.

2.5. Computational methods

Our overall strategy is to use fast, relatively less accurate methods (molecular mechanics conformational searching) to screen for low-energy complex structures, which are then examined using *ab initio* techniques (HF/6-31G*). In general, our calculations used the following protocols. Structures were sketched using the Maestro/Macromodel modeling package (Macromodel version 7.1; Schrödinger Inc.; Portland, OR). Conformational searches were performed using the MMFF94s [15] force field with no nonbonded cutoffs and with conjugate gradient minimization, and using the MCMM search method with automatic setup and 20,000 starting structures.

The lowest-energy structures found in the conformational searches were used as the starting point for both HF/6-31G* and B3LYP/6-31G* full geometry optimizations. These calculations were performed using NWChem (versions 4.7 and 5.0; Pacific Northwest National Laboratory; Richland, WA) [16] and used NWChem default convergence criteria. Molecular symmetry was used to facilitate the calculations where possible. Calculations were set up and monitored using ECCE (versions 3.5 and 4.0; Pacific Northwest National Laboratory; Richland, WA) [17]. VMD (version 1.8.5; University of Illinois at Urbana-Champaign) [18] was used for visualizing molecular structures.

3. Results

3.1. SORI–CID experiments

SORI–CID was carried out by systematically varying the amplitude of the SORI pulse. Relative SORI energies were determined using Eq. (9) to enable comparison of data for the $[H_3N^+(CH_2)_nNH_3^+]$@CB6 complexes as n varies. Disappearance of the parent ions, and appearance of the various fragments, is plotted in Fig. 2 for all the complexes studied.

Disappearance curves for the various complexes are shown in Fig. 3. The falling portions of the curves all have similar slopes except for the $n=4$ data, where too few points were measured to clearly define the fall-off. Relative energies for 50% loss of the parent ion, $E_{SORI,\,50}$, were determined by linear fitting of the falling portion of each disappearance curve, and the energies and standard errors are shown in Fig. 4. For $n=4$, the use of too few points on the falling portion of the curve likely leads to an overestimate of $E_{SORI,\,50}$; comparison with the slopes of the curves for other values of n suggests a value of about 80 would be more appropriate for $n=4$.

We observe three general fragmentation pathways in SORI–CID of $[H_3N^+(CH_2)_nNH_3^+]$@CB6 complexes, illustrated in Scheme 1. These channels include dissociation of the complex by loss of a singly protonated diamine (yielding protonated CB6 as the complementary product; due to mass discrimination in the instrument, protonated CB6 is usually the ion that is observed representing this channel), fragmentation of the CB6 cage, and loss of pieces of the diamine (typically small monoamines) resulting in doubly charged complexes of

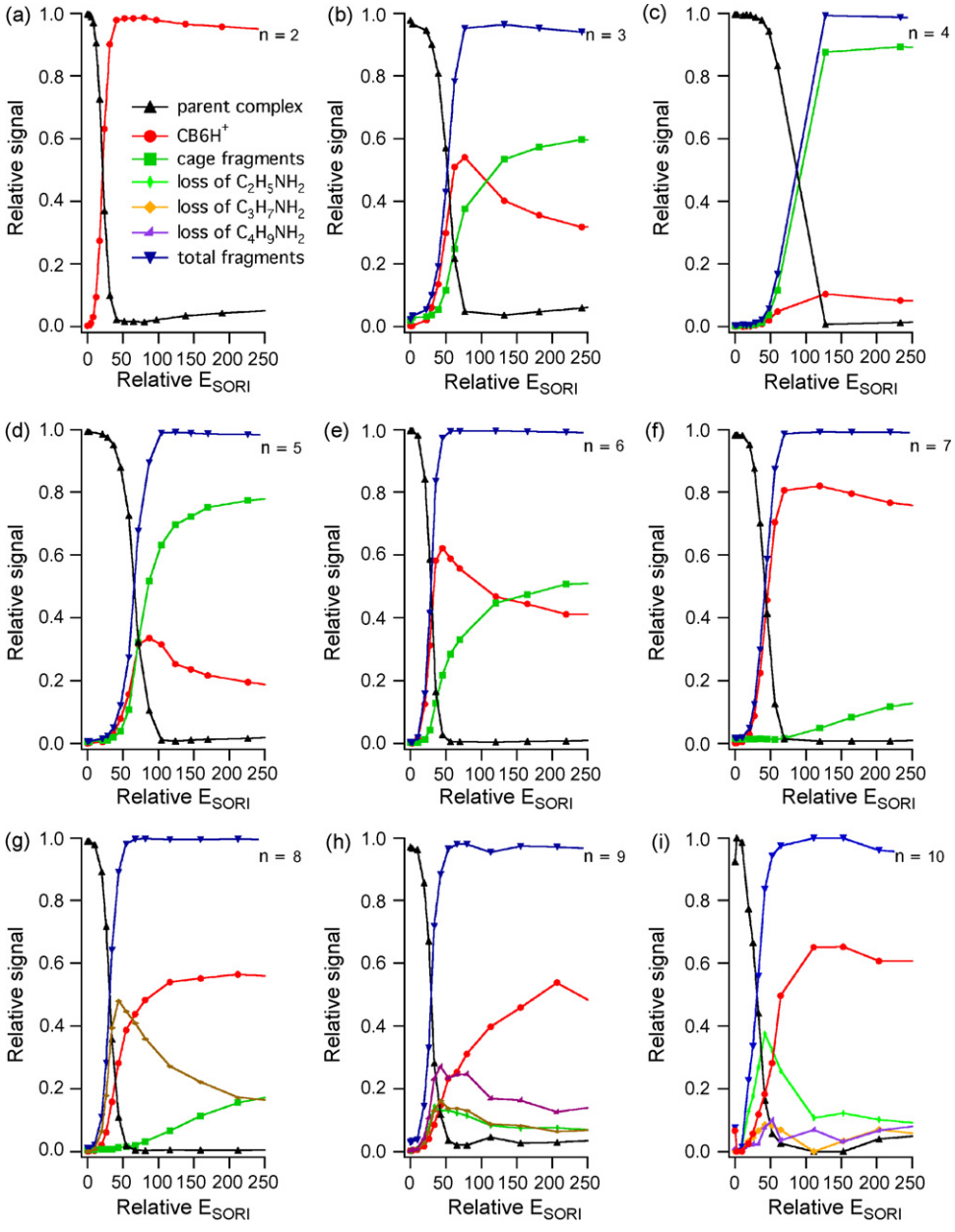

Fig. 2. SORI ion yield curves for $[H_3N^+(CH_2)_nNH_3^+]$@CB6 complexes, $n=2$–10.

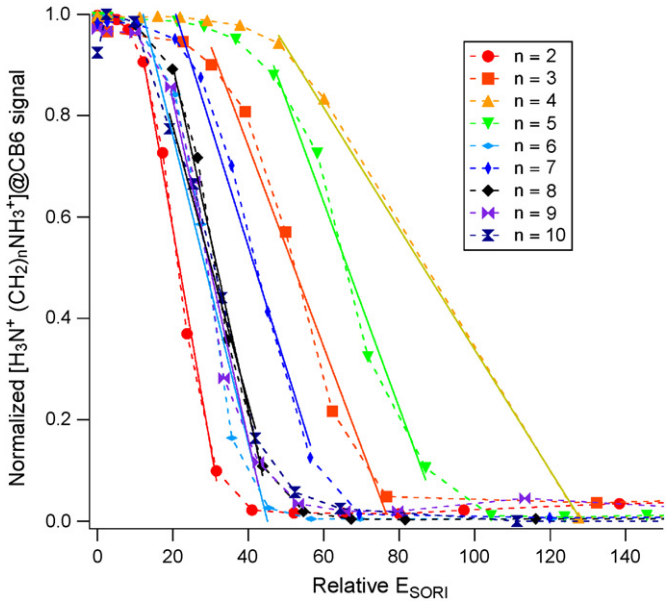

Fig. 3. SORI parent ion survival yield curves for $[H_3N^+(CH_2)_nNH_3^+]$@CB6 complexes, $n = 2$–10. Lines are linear fits used to determine 50% survival for each complex.

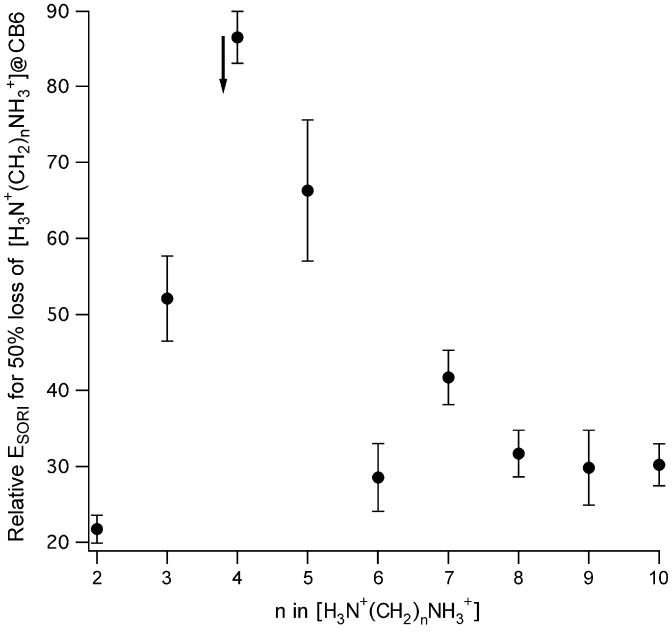

Fig. 4. Relative SORI energies for 50% survival of $[H_3N^+(CH_2)_nNH_3^+]$@CB6 complexes, $n = 2$–10. Error bars represent standard errors from the linear fitting procedure used to derive the values. The arrow at $n = 4$ is to suggest the plotted value is likely too high.

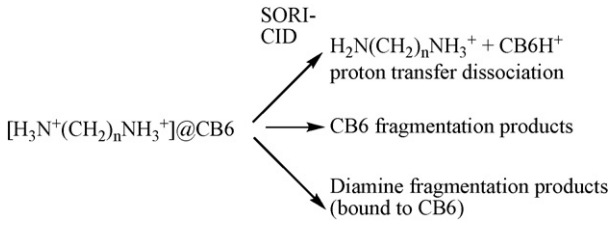

Scheme 1.

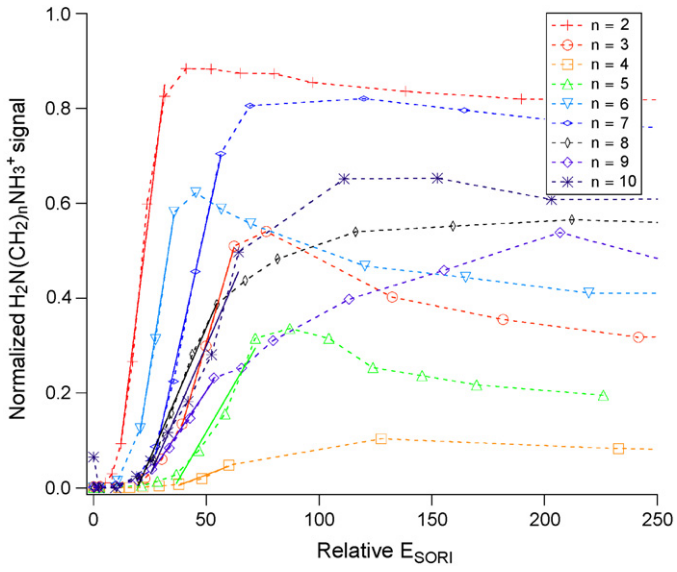

Fig. 5. SORI ion yield curves for production of $CB6H^+$ fragments from $[H_3N^+(CH_2)_nNH_3^+]$@CB6 complexes, $n = 2$–10. Lines are linear fits used to estimate appearance thresholds.

the remaining fragment with CB6. The branching ratios among these three pathways strongly depend on the length of the alkyldiammonium chain, n.

All the complexes exhibit the protonated diamine loss channel (Fig. 2), which is directly compared for all the complexes in Fig. 5. The relative intensity of this channel varies widely with the length of the diamine chain, n, but follows a regular pattern. It is the dominant channel for $n = 2$, is less abundant for $n = 3$, and falls to only about 10% of the SORI products for $n = 4$. For $n = 5$ and $n = 6$ the relative abundance increases, reaching about 80% of all products for $n = 7$. For $n = 8$–10, protonated diamine loss represents up to about 50–60% of the SORI products.

The threshold energies for protonated diamine loss are also of interest. The solid lines in Fig. 5 represent linear fits to the rising portion of the threshold curve that were used to estimate threshold energies. The threshold values, with error bars representing standard errors from the fitting procedure, are shown in Fig. 6 as a function of diamine chain length. The lowest threshold occurs for $n = 2$, with threshold values increasing for $n = 3$ to a maximum for $n = 4$ or 5. The latter two thresholds have large uncertainties because of the relatively low abundance of the protonated diamine loss channel for these complexes. Interestingly, the threshold for $n = 6$ is relatively low, whereas higher, similar values are observed for $n = 7$–10. The protonated diamine loss thresholds shown in Fig. 6 qualitatively parallel the disappearance energies shown in Fig. 4, in that the patterns as n varies are similar.

Cage fragmentation is not observed for $n = 2$, but its relative importance increases with n to a maximum at $n = 4$, concomitant with the minimum abundance of the protonated diamine loss channel (Fig. 2). Cage fragmentation decreases in abundance for $n > 4$, until it is no longer observed for $n > 8$ (Fig. 2h and i).

For the higher values of n, the diamine fragmentation channel increases in importance at the same time as the abundance of cage fragmentation decreases. This is typified by a process corre-

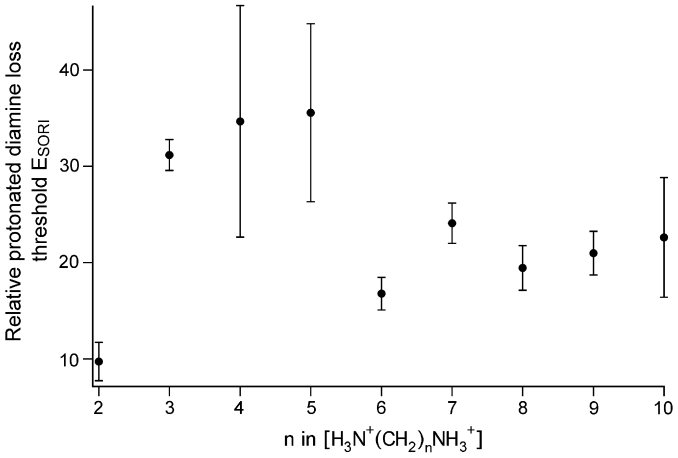

Fig. 6. Relative SORI energies for appearance of $CB6H^+$ fragments from $[H_3N^+(CH_2)_nNH_3^+]$@CB6 complexes, $n = 2$–10. Error bars represent standard errors from the linear fitting procedure used to derive the threshold energies.

sponding to loss of neutral propylamine from the $n = 8$ complex (Fig. 2g). For the $n = 9$ complex, fragmentation corresponding to loss of neutral butylamine is the most prominent diamine fragmentation process (Fig. 2h). Presumably this fragmentation would produce the same ionic complex ion as is formed in propylamine loss from the $n = 8$ complex. For the $n = 10$ complex, the most prominent diamine fragmentation channel corresponds to loss of neutral ethylamine (Fig. 2i), which would yield a doubly charged fragment ion consisting of CB6 and an eight carbon fragment of the original diamine.

3.2. Computational studies

Geometry optimizations were carried out for the doubly protonated complexes of CB6 with each of the diamines, for empty CB6, for singly protonated CB6, and for each of the doubly protonated diammonium ions. CB6 was found to protonate on the carbonyl oxygen rim rather than on one of the glycoluril N atoms; the former structure was more stable than the latter by 106 kJ mol^{-1} at the HF/6-31G* level of theory. The lowest energy conformers of the doubly-protonated diammonium ions were all extended chain structures.

Structures of the various diammonium complexes, optimized at the HF level of theory, are depicted in Fig. 7. All involve threading of the diammonium ion through the CB6 cavity, with hydrogen bonding between the terminal ammonium groups and the carbonyl oxygens of the CB6 rims. Visually, the best match between the length of the diammonium ion and the CB6 cage occurs for $n = 4$–5. For smaller values of n, the diammonium ion is too short to optimally form hydrogen bonds simultaneously with both rims, whereas for larger values the alkyl chain of the diammonium must bend at one or both ends to allow the ammonium groups to reach back to the carbonyl oxygens of the CB6 rims. Typically this bending is asymmetric, occurring to a greater degree at one of the rims than at the other.

Binding of the diammonium ion by CB6 influences the N–N distance in the diammonium ion, which is of interest because this is approximately the charge separation distance in these

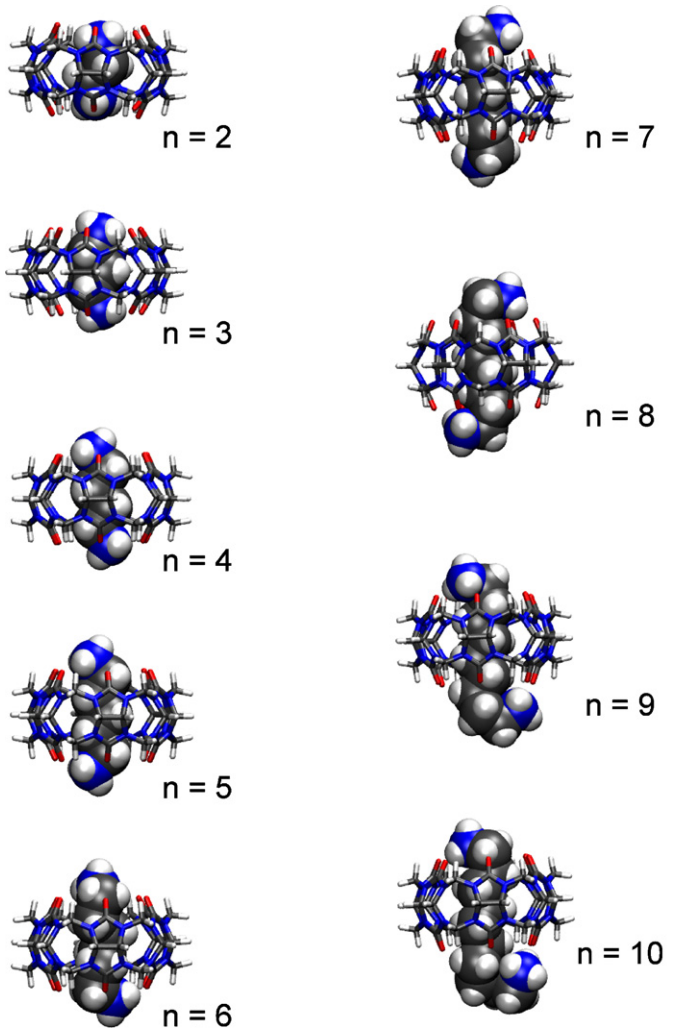

Fig. 7. HF/6-31G* computed structures for $[H_3N^+(CH_2)_nNH_3^+]$@CB6 complexes. Alkyldiammonium ions are represented as space filling models, and CB6 is depicted using tubes.

doubly charged ions. Computed (HF/6-31G*) N–N distances for the doubly-protonated diamines both free in the gas phase and when complexed to CB6 are given in Table 1, along with Coulomb potential energies for the two charges (considered as point charges on the N atoms) calculated using the following equation:

$$E_{\text{Coulomb}} = \frac{q^2}{4\pi\varepsilon_0 d} \tag{10}$$

In Eq. (10), q is the elementary charge, ε_0 is the permittivity of free space (an inaccurate assumption for these complexes, but one that is made for the sake of discussion), and d is the N–N interatomic distance from the HF/6-31G* calculation. For $n = 2$–4, the diammonium N–N distance in the complex is greater than that for the free dication (although only slightly so for $n = 4$), whereas for $n = 5$–9, the distances in the free dications are greater than in the complexed species, especially for $n > 5$. For the larger values of n, the N–N distance in the complexes approaches a constant value of about 9.8 Å.

Table 1
Computed (HF/6-31G*) N–N distances (Å) for free and CB6-complexed diammonium ions, and corresponding electrostatic potential energies (kJ mol^{-1}) for two point charges at those distances

n	N–N		Δ	$E_{Coulomb}$		Δ
	Free diammonium	CB6 complex		Free diammonium	CB6 complex	
2	3.827	3.865	−0.038	363	359	4
3	5.021	5.118	−0.097	277	271	5
4	6.337	6.342	−0.005	219	219	0
5	7.565	7.384	0.181	184	188	−5
6	8.870	7.624	1.246	157	182	−26
7	10.112	8.779	1.333	137	158	−21
8	11.411	9.848	1.563	122	141	−19
9	12.688	9.870	2.818	109	141	−31
10	13.994	9.690	4.304	99	143	−44

Binding energies can be derived from the computed energies of the complexes and their components. Experimentally, we observed dissociation of each of the complexes by loss of a singly-protonated diamine accompanied by proton transfer to CB6. Computationally, this process was modeled by calculating the energies of the complex and of the protonated diamine and protonated CB6 dissociation products.

Table 2
Computed enthalpies (kJ mol^{-1}) for binding singly-protonated α,ω-alkyldiammonium guests to singly-protonated CB6 hosts

n	D[$H_2N(CH_2)_nNH_3^+$-CB6H$^+$]	
	HF/6-31G*	B3LYP/6-31G*
2	−129	−131
3	−190	−170
4	−229	−204
5	−252	−229
6	−240	−228
7	−231	−226
8	−228	−221
9	−208	−201
10	−185	−181

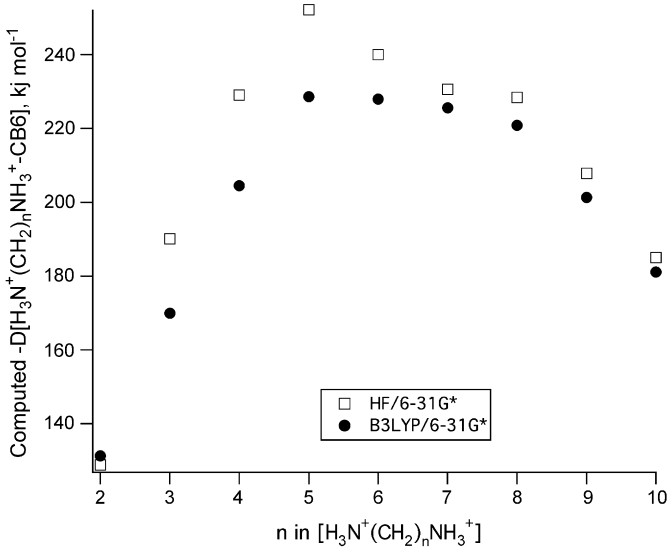

Fig. 8. Computed dissociation energies for $[H_3N^+(CH_2)_nNH_3^+]$@CB6 → $H_2N(CH_2)_nNH_3^+ + CB6H^+$.

Computed energies, derived from HF/6-31G* and B3LYP/6-31G* geometry optimizations, are given in Table 2. The reported energies have not been corrected for zero point energies (because of the difficulty in performing vibrational calculations for systems of this size) or for basis set superposition error (because it is not clear that such corrections are important when comparing relative energies of such similar, homologous complexes). For the proton transfer process, the HF/6-31G* and B3LYP/6-31G* results (shown graphically in Fig. 8) are in reasonably good agreement, with the HF results generally slightly greater than the B3LYP results. Both sets of calculations indicate the lowest binding energy for $n = 2$, the greatest binding for $n = 5$, and gradually decreasing energies for $n > 5$.

4. Discussion

4.1. Optimum α,ω-diammonium chain length for CB6 binding

In aqueous formic acid solution, the maximum binding constant for alkyldiamines interacting with CB6 occurs for $n = 6$ [4,19]. However, the solution binding constant is likely influenced by solvation, and may not relate directly to the structures of the binding partners. In fact, the nitrogen atoms in the energetically favored extended conformation of hexanediammonium are about 7.5 Å apart (center to center; see Table 1), which is significantly greater than the height of CB6 (about 6.14 Å, measured as the distance between corresponding oxygen atoms in opposite rims). The best length match occurs for $n = 4$, with an N–N distance of 6.34 Å. Is there an optimum diammonium chain length for binding CB6, and if so, what is it?

The gas phase is the best environment for finding answers to these questions, because only in the gas phase can the questions be addressed directly without the perturbing influence of neighboring atoms. Several pieces of data suggest the optimal length occurs for $n = 4$. As noted above, based on purely geometric considerations from the computational studies, the $n = 4$ diammonium ion is the best match to the height of the CB6 cage. This chain length is also the one for which the complex disappearance energy, $E_{SORI,\,50}$ (Fig. 4), is maximum. The $E_{SORI,\,50}$ values may be taken as indicators of the overall relative stabilities of the various complexes, so it is clear that the $n = 4$ complex is

the most robust of those studied. For $n=4$ the proton transfer dissociation channel has the lowest relative signal (Figs. 2 and 5), and cage fragmentation represents the greatest fraction of the overall signal (about 90%). The energy required to cause cage fragmentation should not vary a great deal as alkyldiammonium chain length is varied. Therefore, at $n=4$ the proton transfer dissociation channel does not compete effectively with cage fragmentation, suggesting it is easier to disrupt the CB6 cage than to remove the protonated diamine from the cavity. Finally, the proton transfer dissociation threshold is greatest for $n=4$ (along with $n=5$, which has a similar value; Fig. 6).

On the other hand, the computed proton transfer binding energies suggest that the optimum α,ω-diammonium chain length for CB6 binding in the gas phase is five carbon atoms. These energies are about 20 kJ mol^{-1} greater for $n=5$ than for $n=4$ at both HF and B3LYP levels of theory (Table 2 and Fig. 8). The most likely explanation for the difference between computed binding energies and the experimental threshold data is that these two methods probe different features of the potential energy surface leading to dissociation. The computed binding energies reflect the energetic difference between a fully relaxed complex and fully relaxed products, whereas the experimental threshold data probe the activation barriers for dissociation. These values will only be the same for reactions with no reverse activation barrier, and such is certainly not the case for the dissociation reactions probed here. At minimum the two charges present a Coulomb barrier to the reverse, association reaction. A rough estimate of the magnitude of the Coulomb barrier to association is given in the electrostatic potential energies listed in Table 1 for the CB6 complexes. These values, which are the energies required to bring two point charges from infinite separation to the distances calculated for the ammonium nitrogen atom separation in the supramolecular complexes, are quite large (ranging from 359 kJ mol^{-1} for the complex of the $n=2$ diamine down to around 140 kJ mol^{-1} for $n=8$–10). Computational methods for more accurately determining the dissociation barriers are available, but require calculation of the potential surface along the dissociation channel to locate the top of the barrier. Such calculations would be quite challenging for systems as large as those examined here, and we have not attempted them. However the good news is that the computational and experimental results are probably not actually in conflict at all.

In summary, $n=4$ is most likely the optimum chain length for CB6 binding in the gas phase. It is reasonable to expect a smaller optimum length in the gas phase than was found in solution ($n=6$), because in solution the ammonium charges can be stabilized by the solvent as well as by the CB6 cage. Therefore, protrusion of the α,ω-diammonium ion out of the cage and into the solvent is favorable, favoring longer chain lengths than in the gas phase, where such stabilization is not possible.

4.2. Complexed α,ω-diammonium ions as "molecular springs"

Both the $E_{SORI,\,50}$ and protonated diamine loss threshold values are low for the $n=6$ complex in comparison to the neighboring complexes. This raises the question of what is special about the $n=6$ complex to cause such experimental results, especially when the computed binding energies for $n=6$ seem to fit a regular pattern with $n=4$, $n=5$, and $n=7$; computationally, the values for $n=6$ are not especially low and do not particularly stand out.

Reference to Table 1 suggests the geometry of the $n=6$ complex is somewhat unique. For $n<6$, the N–N distances in the free diammonium ions are similar to those in the corresponding complexed diammonium ions, with differences all less than 0.2 Å. For $n=6$, complexation draws the two nitrogen atoms much closer together than they are in the free α,ω-diammonium cation, by about 1.2 Å. This is achieved by bending the alkyl chain on one end to allow the terminal ammonium greater proximity to the CB6 rim (Fig. 7); the $n=6$ diammonium cation is the only one with a single bend when complexed to CB6.

For two point charges in free space, this change in distance due to bending corresponds to 26 kJ mol^{-1} greater electrostatic potential energy. Charge delocalization and the intervening atoms probably make the effect smaller for the complex than it would be for point charges in free space, but in a sense the hexanediammonium ion in the complex is like a loaded spring; perhaps this contributes to the relative ease with which this complex dissociates.

It is important to remember that whereas the computational studies probe the overall energetics of the dissociation reactions, the SORI experiments probe the activation barriers. Overall reaction energetics directly correspond to reaction barriers only for reactions with no reverse activation barrier; the dissociation reactions discussed here are not barrier-free. The fact that the thresholds are low for dissociation of the $n=6$ complex, whereas the overall energetics are not, suggests that dissociation of the $n=6$ complex is kinetically different from its neighboring homologues. The single bend near one end of the alkyl chain in the $n=6$ complex very likely means the two ends of the diammonium ion are not attached to CB6 with identical binding energies. Mechanistically, it is possible that one end of the chain is significantly more easily detached than the other, shifting the position of the transition state and lowering the activation energy, and supplying a plausible explanation for the unusually low threshold energies for this complex.

For $n>6$, the alkyl chains each have two bends, and likely are bound more symmetrically. The $n=7$ and 8 complexes are long enough and inflexible enough that their change in electrostatic repulsion upon complexation is less than for $n=6$. The $n=9$ and 10 complexes are significantly more compressed geometrically than $n=6$, but apparently relieve this electrostatic strain through diamine fragmentation rather than through loss of protonated diamine from the complex. It may be possible to exploit these "molecular spring" effects in future molecular machines.

4.3. Quantification of SORI threshold data

Because of the relative ease with which SORI experiments can be performed, their applicability to larger molecular systems, and their wide use, it is highly desirable to develop these methods for quantitative thermochemistry. SORI-CID differs from traditional threshold CID [7,20,21] in at least two important

ways. First, SORI is inherently a multiple-collision technique, in which energy is added to the ion through a series of low energy collisions rather than in a single high-energy collision. This adds ambiguity to the energy scale, and is probably the principal reason quantitative SORI has not been widely practiced. In addition, the stepwise nature of ion activation means that the lowest-energy dissociation channels are selectively populated, discriminating against higher energy channels [7]. Second, the time scale for SORI experiments is much longer (ms to s) than that for single collision CID experiments (μs). This is advantageous for SORI because it means SORI experiments are much less subject to kinetic shifts in threshold, and therefore can be applied to much larger molecular systems than traditional CID methods with less need for large kinetic shift corrections.

Collision induced dissociation threshold techniques are well established for obtaining quantitative thermochemical information [20,21]. Threshold CID experiments are carefully controlled so the kinetic energy in the center-of-mass reference frame is well known prior to collision and single collision conditions overwhelmingly dominate; under multiple collision conditions, knowledge of the collision energy for all collisions but the first is lost, making it difficult to determine how much energy is collisionally deposited.

By its nature, SORI is a multiple collision technique. Under SORI conditions, ions undergo many low energy collisions with background gas, gradually adding energy until the dissociation threshold is reached. Energy deposition during the SORI process has been characterized for several small molecule systems [13,14] and for biomolecules [12,22]. SORI is routinely used in many laboratories to cause dissociation of peptides and proteins, but has not been widely used to obtain quantitative thermochemistry. By carefully modeling the collisional energy deposition function and using the results to fit the experimental fragmentation curves, Laskin and Futrell have successfully used SORI to quantitatively characterize the dissociation of bromobenzene [14] and bromonaphthalene [13] ions, obtaining good agreement with values obtained by other methods. Using pump-probe techniques, Heeren's group was able to quantify the amount of energy deposited into leucine enkephalin ions during each SORI cycle, and to show that infrared cooling of the ions was a significant energy loss mechanism at low ambient temperatures during SORI [12].

To make the SORI results quantitative, energy must be added to the ions in a measurable way until dissociation is observed, and the measured quantities must then be related to the binding energies we desire to determine. Energy deposition can be varied by varying the amplitude of the off-resonant RF waveform (as was done in this study), by varying the difference between the applied frequency and the ions' resonant frequency, by varying the duration of the SORI event, or by varying the pressure and/or mass of the background gas. Heeren's work [12] makes a strong case that the best way to vary SORI energy deposition is by varying the length of the SORI event, rather than varying the amplitude as we have done. Heeren's approach removes possible ambiguities about variation of energy deposition with changes in average kinetic energy, at the expense of being slightly more difficult to implement experimentally; we plan to use this approach in the future.

Although we have made no attempt to calibrate and quantify the SORI energy scale, the results from the work of Laskin and Futrell, and those from Heeren's group, suggest that this should be possible. Similarly, the results of this study give qualitative trends in dissociation energy that are reproducible and in accord with expectations, bolstering the idea that quantitative SORI is possible in principle.

5. Conclusions

The results presented in this study have significant implications for both the supramolecular chemistry community and the mass spectrometry community, which unfortunately are usually separate groups.

For supramolecular chemists, we have attempted to show that energy-resolved SORI-CID will likely prove to be a powerful addition to the arsenal of characterization techniques for supramolecular complexes in the gas phase. Specifically, we have demonstrated that α,ω-alkyldiammonium binding by CB6 is optimum for a shorter alkyldiammonium chain in the gas phase than in solution, which is reasonably interpreted in terms of solvation of the ends of the chain by bulk solvent that is not present in the gas phase environment. The work further suggests that compressed alkyldiammonium "molecular springs" might be detectable via tandem mass spectrometric methods.

Two key messages emerge for mass spectrometrists. First, more work is needed to make SORI-CID a more powerful tool. The next important step in the development of SORI-CID as a characterization method will be to add quantitation so that it can be used to obtain quantitative thermochemical information. Second, this work provides another example of the synergy that is possible between theory and experiment, even for supramolecular systems that are somewhat larger than the small molecules gas phase chemists typically examine. HF and B3LYP calculations using the 6-31G* basis set are generally consistent with the experiments and provide valuable data to complement the experimental work, while the agreement with experiment also increases our confidence in the computational results.

Acknowledgments

We are grateful for computer time and support from the Ira and Marylou Fulton Supercomputing Center at Brigham Young University, and for financial support from the National Science Foundation (CHE-0615964).

References

[1] D.E. Newton, Recent Advances and Issues in Molecular Nanotechnology, Greenwood Press, Westport, CT, 2002.
[2] R.D. Smith, J.A. Loo, R.R.O. Loo, M. Busman, H.R. Udseth, Mass Spectrom. Rev. 10 (1991) 359.
[3] M. Mann, M. Wilm, Trends Biochem. Sci. 20 (1995) 219.
[4] W.L. Mock, Cucurbituril, in: F. Vögtle (Ed.), Comprehensive Supramolecular Chemistry, vol. 2, Elsevier, New York, 1996.

[5] H. Zhang, E.S. Paulsen, K.A. Walker, K.E. Krakowiak, D.V. Dearden, J. Am. Chem. Soc. 125 (2003) 9284.
[6] J.W. Gauthier, T.R. Trautman, D.B. Jacobson, Anal. Chim. Acta 246 (1991) 211.
[7] J. Laskin, J.H. Futrell, Mass Spectrom. Rev. 24 (2005) 135.
[8] M.W. Senko, J.D. Canterbury, S. Guan, A.G. Marshall, Rapid Commun. Mass Spectrom. 10 (1996) 1839.
[9] M. Wigger, J.P. Nawrocki, C.H. Watson, J.R. Eyler, S.A. Benner, Rapid Commun. Mass Spectrom. 11 (1997) 1749.
[10] L. Chen, T.-C.L. Wang, T.L. Ricca, A.G. Marshall, Anal. Chem. 59 (1987) 449.
[11] C.Q. Jiao, D.R.A. Ranatunga, W.E. Vaughn, B.S. Freiser, J. Am. Soc. Mass Spectrom. 7 (1996) 118.
[12] X. Guo, M.C. Duursma, A. Al-Khalili, R.M.A. Heeren, Int. J. Mass Spectrom. 225 (2003) 71.
[13] J. Laskin, J. Futrell, J. Phys. Chem. A 104 (2000) 5484.
[14] J. Laskin, M. Byrd, J. Futrell, Int. J. Mass Spectrom. 195/196 (2000) 285.
[15] T.A. Halgren, J. Comput. Chem. 17 (1996) 490.
[16] E. J. Bylaska, W. A. de Jong, K. Kowalski, T. P. Straatsma, M. Valiev, D. Wang, E. Apra, T. L. Windus, S. Hirata, M. T. Hackler, Y. Zhao, P.-D. Fan, R. J. Harrison, M. Dupuis, D. M. A. Smith, J. Nieplocha, V. Tipparaju, M. Krishnan, A. A. Auer, M. Nooijen, E. Brown, G. Cisneros, G. I. Fann, H. Fruchtl, J. Garza, K. Hirao, R. Kendall, J. A. Nichols, K. Tsemekhman, K. Wolinski, J. Anchell, D. Bernholdt, P. Borowski, T. Clark, D. Clerc, H. Dachsel, M. Deegan, K. Dyall, D. Elwood, E. Glendening, M. Gutowski, A. Hess, J. Jaffe, B. Johnson, J. Ju, R. Kobayashi, R. Kutteh, Z. Lin, R. Littlefield, X. Long, B. Meng, T. Nakajima, S. Niu, L. Pollack, M. Rosing, G. Sandrone, M. Stave, H. Taylor, G. Thomas, J. van Lenthe, A. Wong, Z. Zhang, NWChem, A Computational Chemistry Package for Parallel Computers, ver. 5.0, (2006).
[17] G. Black, B. Didier, D. Feller, D. Gracio, M. Hackler, S. Havre, D. Jones, E. Jurrus, T. Keller, C. Lansing, S. Matsumoto, B. Palmer, M. Peterson, K. Schuchardt, E. Stephan, H. Taylor, G. Thomas, E. Vorpagel, T. Windus, C. Winters, Ecce, A Problem Solving Environment for Computational Chemistry, ver. 3.1, 2003.
[18] W. Humphrey, A. Dalke, K. Schulten, J. Mol. Graphics 14 (1996) 33–38.
[19] W.L. Mock, N.-Y. Shih, J. Org. Chem. 51 (1986) 4440.
[20] P.B. Armentrout, Collision-induced dissociation, in the encyclopedia of mass spectrometry, in: P.B. Armentrout (Ed.), Theory and Ion Chemistry, vol. 1, Elsevier, San Diego, 2003.
[21] P.B. Armentrout, Reaction threshold energy measurements, the encyclopedia of mass spectrometry, in: P.B. Armentrout (Ed.), Theory and Ion Chemistry, vol. 1, Elsevier, San Diego, 2003.
[22] P.D. Schnier, J.C. Jurchen, E.R. Williams, J. Phys. Chem. B 103 (1999) 737.